RSC Advances

Cite this: *RSC Advances*, 2012, **2**, 5205–5213

www.rsc.org/advances

PAPER

Size-dependent phase transitions in nanostructured zirconia–scandia solid solutions†

Paula M. Abdala,*[ab] Aldo F. Craievich[c] and Diego G. Lamas[d]

Received 20th March 2012, Accepted 21st March 2012
DOI: 10.1039/c2ra20512b

The dependences of phase stability and solid state phase transitions on the crystallite size in ZrO_2-10, 12 and 14 mol% Sc_2O_3 nanopowders are investigated by X-ray powder diffraction using a synchrotron source (S-XPD). The average crystallite sizes lie within the range of 35 to 100 nm, approximately. At room temperature these solid solutions were previously characterised as mixtures of a cubic phase and one or two rhombohedral phases, β and γ, with their fractions depending on composition and average crystallite sizes. In this study, it is shown that at high temperatures these solid solutions become cubic single-phased. The size-dependent temperatures of the transitions from the rhombohedral phases to the cubic phase at high temperature are determined through the analyses of a number of S-XPD patterns. These transitions were studied on cooling and on heating, exhibiting hysteresis effects whose relevant features are size and composition dependent.

1. Introduction

Over the last few years, size effects on phase stability and phase transitions in technologically relevant materials have received growing attention. A number of previous investigations reported that unusual crystalline phases appear in oxide, metallic or ceramic nanomaterials at room temperature, these phases generally corresponding to the high temperature polymorph of the same material in bulk state. Additionally, size-dependent shifts in the transition temperatures for on heating or on cooling cycles were observed.[1–12]

The knowledge of the relationships between crystallite size, phase content and physical properties of nanopowders can lead to the development of material tailoring processes through an adequate control of the crystallite size. Thus, the quantitative characterization of size effects on phase stability and related structural changes in ceramic materials is not only relevant from a scientific point of view but also because of their related technological consequences. It is well known that the different features of the structure of ZrO_2-based materials strongly affect their properties. Particularly, for technological applications in solid oxide fuel cells (SOFCs) or in gas sensors, ZrO_2 is commonly doped with oxides of aliovalent cations such as Y_2O_3 or CaO. In these solid solutions, the dopant stabilizes the cubic phase – which is stable only at high temperatures in undoped ZrO_2 – down to room temperature. The added oxide creates ion vacancies in the ZrO_2 host lattice, thus increasing the oxygen-ion electric mobility.[13]

ZrO_2–Sc_2O_3 (zirconia–scandia) solid solutions are known to exhibit very high oxygen ion conductivity provided their structure is composed of cubic and/or pseudocubic tetragonal phases.[14] These materials also have the same excellent mechanical and chemical stabilities as other ZrO_2-based solid solutions, making them good candidates for electrolytes in intermediate-temperature SOFCs. In spite of these advantages, for solid ZrO_2–Sc_2O_3 polycrystalline samples with typical micrometrical average crystal sizes, the high conductivity cubic phase is only stable above 600 °C. Depending on composition, three rhombohedral phases, named as β, γ and δ, with low ionic conductivity are stable below 600 °C down to room temperature, within the compositional range of interest for SOFCs. The features of the transitions between these phases are quite complex and not yet fully understood.[15–17]

In compositionally homogeneous ZrO_2-based systems, the tetragonal phase can exhibit three forms, known as t, t′ and t′′. The stable tetragonal form is called the t-form. The t′ and t′′ forms are defined as compositionally homogeneous metastable phases. In the t′-form the axial ratio, *c*/*a*, is larger than unity. The t′′-form has an axial ratio, *c*/*a*, of unity with the oxygen atoms displaced along the *c* axis from their ideal sites of the cubic phase.[13]

[a]*Swiss-Norwegian Beam Lines, European Synchrotron Radiation Facility, 6 rue Jules Horowitz, 38043, Grenoble, France. E-mail: abdala@esrf.fr; Fax: +33 4 76 88 26 94; Tel: +33 4 76 88 29 02*
[b]*CINSO (CONICET-CITEDEF), J.B. de La Salle 4397 (1603) Villa Martelli, Pcia de Buenos Aires, Argentina*
[c]*Instituto de Física, FAP, USP, Travessa R da Rua do Matão, no.187, Cidade Universitária, São Paulo, Brazil 05508-900. E-mail: craievich@if.usp.br*
[d]*Laboratorio de Caracterización de Materiales, Facultad de Ingeniería, Universidad Nacional del Comahue, Buenos Aires 1400, (8300) Neuquén Capital, Pcia. de Neuquén, Argentina and CONICET, Argentina. E-mail: diego.lamas@fain.uncoma.edu.ar*
† Electronic Supplementary Information (ESI) available. See DOI: 10.1039/c2ra20512b

A remarkable feature of ZrO_2–Sc_2O_3 materials is that the crystallite size in the nanometric range plays a significant role in the stability of the different cubic, tetragonal and rhombohedral phases.[18–20] Our previous investigations on nanocrystalline and compositionally homogeneous ZrO_2-1 to 14 mol% Sc_2O_3 solid solutions with an average crystallite under 35 nm indicated the presence of a single cubic or tetragonal phase over the whole compositional range, at room temperature.[19,20] On the contrary, samples with Sc_2O_3 contents between 10 and 14 mol% with larger crystallite sizes, with average size $<D> > 35$ nm, exhibit a mixture of a cubic (or pseudo-cubic tetragonal t′′) phase at room temperature coexisting with rhombohedral phases (β and γ), the content of these rhombohedral phases increasing for increasing average crystallite size.[20]

The knowledge of crystallite size effects on solid–solid phase transitions is expected to be useful in order to understand the mechanisms involved in the phase stability of the studied materials. Previous authors studied the size dependence corresponding to the monoclinic–tetragonal phase transition in ZrO_2 based systems.[1,7,21,22] Nevertheless, the β-cubic and γ-cubic phase transitions were not previously reported.

This work aims at determining the dependence on the crystallite size of the solid state phase transition as a function of the temperature in nanostructured ZrO_2–Sc_2O_3 solid solutions with average crystallite sizes $<D> \geqslant 35$ nm. These features are here investigated by synchrotron X-ray powder diffraction (S-XPD) as functions of (i) the material composition within the range 10 to 14 mol% Sc_2O_3, (ii) the average crystallite sizes over the range from 35 nm up to 105 nm, and (iii) the temperature, from room temperature up to 900 °C. S-XPD measurements allowed us to distinguish between the different, and in many cases coexisting, rhombohedral and cubic polymorphs, and quantify the content, which is not easily achieved by using other techniques.[15,16]

2. Experimental section

ZrO_2–Sc_2O_3 nanopowders were synthesized by the gel-combustion method using a nitrate–lysine route and treated at 935, 1000 and 1200 °C to yield different crystallite sizes. The experimental details of the sample preparation and structural characterization at room temperature of these nanopowders were described in previous works.[19,20]

S-XPD experiments were carried out at the D10B-XPD beam line of the Brazilian National Synchrotron Light Laboratory (LNLS), Campinas, Brazil, using a monochromatic beam with a wavelength $\lambda = 1.5498$ Å. A furnace mounted on the powder diffractometer enabled S-XPD measurements from room temperature up to 900 °C. The experiments were performed under heating and cooling conditions at heating/cooling rates of 5 °C min^{-1}. The temperature was measured with a thermocouple placed close to the sample and previously calibrated by using XPD patterns of a MgO standard measured at different temperatures.

S-XPD data were collected using a symmetric θ–2θ scanning geometry. Two extended X-ray patterns of all samples, within a $20° < 2\theta < 100°$ range, were recorded at room temperature and at high temperature (800 or 900 °C depending on the composition). In order to follow the phase contents as functions of temperature, many consecutive S-XPD patterns were recorded over the 2θ ranges close to the 111 or the 220 Bragg peaks of the cubic or tetragonal structures. In this way, the cubic and the rhombohedral, β and γ, phases were clearly distinguished.

A high-intensity and moderate resolution configuration – *i.e.* without using a crystal analyzer – was employed for these S-XPD measurements.[19,23] This configuration provides a high photon flux allowing for good counting statistics using a very short acquisition time, while the results are not affected by the inherent low resolution because the Bragg peaks of nanomaterials are intrinsically broad.

The discrimination between the cubic phase with a fluorite-type structure and the pseudo-cubic t′′-form of the tetragonal phase detected in some of the studied samples was achieved by measuring the X-ray scattering intensity over a small 2θ range close to the 112 Bragg reflection at room temperature and at high temperature.[18,20] This reflection, forbidden for a fcc crystal structure, is expected to be non-vanishing for crystalline powders with oxygen atoms displaced from their ideal sites in the fluorite-like cubic lattice. For example, the quantitative evaluation of these "forbidden" peaks is used to discriminate between the cubic and pseudo-cubic t′′ phases, since the t′′ phase exhibits a cubic unit cell but with a tetragonal symmetry due to the displacement of oxygen atoms. As described elsewhere, the use of a synchrotron X-ray beamline for the measurement of powder diffraction patterns allows the detection and precise measurement of this weak reflection.[18–20]

The weight fractions of the different component phases were calculated as functions of temperature using the single line method. This procedure is based on the determination of the ratio between the intensity of a Bragg peak in the mixture and that of the same peak in a single-phased sample.[24] For the calculations of the integrated intensities by the single line method, the fitting of the Bragg peak was performed using the FullProf Suite program.[25]

The average crystallite sizes of the samples, $<D>$, were determined for the high temperature cubic or pseudo-cubic phase from the width of the 111 Bragg peak by applying the Scherrer equation.[24] We have preferred to determine the average crystallite sizes from the analysis of the high temperature S-XPD patterns because this procedure is easier than the analysis of room temperature patterns since, at high temperature, the samples are single-phased. The instrumental broadening was determined from the analysis of a LaB_6 standard (NIST-SRM 660a).

3. Results

3.1. Structure of ZrO_2–Sc_2O_3 nanopowders at room temperature

Our previous Rietveld analyses of S-XPD patterns of ZrO_2–Sc_2O_3 materials at room temperature, for three different sample compositions and three average crystallite sizes, led to the phase compositions that are listed in Table S1 in the ESI.[20] The average crystallite sizes corresponding to the high-temperature cubic phase determined from S-XPD patterns are given in Table S1 in the ESI, while those corresponding to the phases observed at room temperature were reported in a previous publication.[20] Nanopowders corresponding to each of the three different compositions, 10, 12 and 14 mol% Sc_2O_3, were calcined at 935 °C, 1000 °C and 1200 °C, yielding for all compositions a

similar set of average sizes, $<D>$, within the ranges 35–40 nm, 60–65 nm and 90–105 nm, respectively.

ZrO_2-10 mol% Sc_2O_3 samples exhibit a binary mixture of pseudo-cubic t′′ and rhombohedral β phases, with a decreasing content of β phase for decreasing average crystallite size. The ZrO_2-12 mol% Sc_2O_3 solid solutions contain a mixture of cubic (c), rhombohedral β and rhombohedral γ phases, with their respective phase contents also depending on the average crystallite size. Finally, the ZrO_2-14 mol% Sc_2O_3 samples mainly contain c and γ phases, and a minor fraction of β phase (12 wt% or less).

Our previous results also indicated that nanostructured ZrO_2–Sc_2O_3 solid solutions with very small average crystallite sizes ($<D> < 35$ nm) totally retain the high temperature c phase down to room temperature, or the pseudo-cubic t′′ form, without any trace of rhombohedral phases.[19,20]

All powders studied here are composed of nanocrystals with a rather wide size distribution. As a matter of fact, the quotients between the standard deviation σ and the average size value $<D>$, determined for a set of five of our samples by $FW_{1/5}/_{4/5}$, range from 0.2 up to 0.5, with an average value $\sigma/<D> = 0.4$.[26] Further information on the size distribution analysis has been provided in the ESI (Fig. S1).

Thus, for powders with average crystallite sizes larger than the upper critical size (*i.e.* $<D> > 35$ nm), a noticeable fraction of the crystallites have sizes smaller than the critical size, $D < 35$ nm.[6,18–20] This implies that, for decreasing average crystallite size, the fractions of c or t′′ phases are expected to progressively increase.

The arguments mentioned in the previous paragraphs clearly indicate that the presence of cubic or tetragonal phases, with their volume fractions increasing with decreasing $<D>$, together with one or two rhombohedral phases can safely be assigned to the existence of crystallites with sizes smaller than the critical upper size.

The volume fraction corresponding to very small crystallites with cubic or pseudo-cubic phases observed at room temperature is expected to remain essentially invariant through the whole heating/cooling temperature cycling. This implies that the rhombohedral-to-cubic transition by heating and the reversal cubic-to-rhombohedral by cooling do not involve the whole sample volume.

3.2. Structural characterization of ZrO_2–Sc_2O_3 solid solutions at high temperature

Fig. 1a displays the full S-XPD pattern corresponding to the ZrO_2-10 mol% Sc_2O_3 sample with an average crystallite size $<D> = 35$ nm held at 800 °C. All Bragg peaks were indexed assuming a face centered cubic (fcc) unit cell. Similar diffractograms were obtained for samples of average crystallite sizes $<D> = 60$ and 100 nm. As it is shown in the S-XPD profiles displayed in Fig. 1b, no splitting of the 400 peak was observed for any of the three ZrO_2-10 mol% Sc_2O_3 samples, showing in all cases cell parameters $a = c$. This confirms that their unit cells are cubic and their cations are located in sites with cubic symmetry.

As explained above, there are two types of phases observed in ZrO_2-based solid solutions that exhibit a cubic unit cell, namely the c phase (fcc fluorite-type structure) and the t′′-form of the

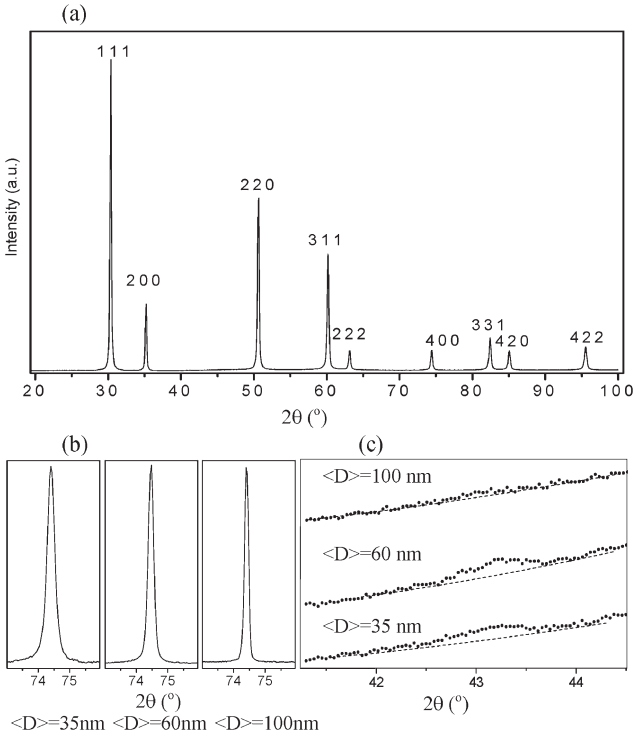

Fig. 1 Results of S-XPD measurements for ZrO_2-10 mol% Sc_2O_3 nanopowders held at 800 °C. (a) XPD pattern corresponding to a nanopowder with an average crystallite size of $<D> = 35$ nm. All peaks were indexed according to a fluorite-type structure (fcc unit cell). Additional very weak Bragg reflections forbidden for fluorite-type structures (not visible in this pattern) were detected. (b) S-XPD profiles of the (400) Bragg peak for different average crystallite sizes, $c = a = 5.129(9)$. (c) S-XPD patterns measured over the 2θ range near to the 112 Bragg peak corresponding to nanopowders with different average crystallite sizes.

tetragonal phase, *i.e.* a cubic unit cell with the oxygen atoms displaced from the expected positions in the fluorite-type structure. In order to discriminate between these two similar structures, a more careful study of the S-XPD patterns was required by monitoring the integral intensity of a weak Bragg peak (such as 112) related to the displacement of oxygen atoms.

Fig. 1c displays the S-XPD patterns for nanopowders with 10 mol% Sc_2O_3 content, over the 2θ range close to the 112 peak corresponding to samples with different crystallite sizes. This reflection is clearly apparent in the S-XPD patterns corresponding to samples with average crystallite sizes $<D> = 35$ and 60 nm, while this reflection vanishes, or is extremely weak, in the pattern associated to the powder with $<D> = 100$ nm. The very weak, almost vanishing, 112 Bragg peak of S-XPD patterns of the ZrO_2-10 mol% Sc_2O_3 nanopowder (Fig. 1c) indicates that the phase corresponding to the solid solution with the largest crystallite average size, $<D> = 100$ nm, exhibits a cubic unit cell with an essentially fluorite-like structure, in agreement with previous studies of ZrO_2-10 mol% Sc_2O_3 solid solutions composed of larger (micrometric) crystallites.[15]

For ZrO_2-10 mol% Sc_2O_3 nanopowders with average crystallite sizes $<D> = 35$ and 60 nm, the 112 peak is clearly apparent (Fig. 1c) thus indicating that the structure corresponds to the

t′′-form of a tetragonal phase. As has been demonstrated in our previous studies, the t′′-form can be fully retained down to room temperature in nanocrystalline solid solutions with small average crystallite sizes ($<D> < 35$ nm).[18–20]

In all S-XPD patterns recorded at high temperatures corresponding to ZrO_2-12 mol% Sc_2O_3 and ZrO_2-14 mol% Sc_2O_3 solid solutions, with different average crystallite sizes, the 112 Bragg peak was absent. These results indicate that all nanopowders with 12 and 14 mol% Sc_2O_3 exhibit a cubic fluorite-type structure.

We concluded that ZrO_2–Sc_2O_3 nanopowders with 10, 12 and 14 mol% Sc_2O_3 and average crystallite sizes $<D>$ of 35, 60 and 100 nm, held at high temperature (above $T \approx 600$ °C), exhibit a crystal structure with a cubic unit cell. All of them exhibit a fluorite-type structure except those with the lowest composition (10 mol% Sc_2O_3) and smallest crystallite average sizes ($<D>$ = 35 and 60 nm), which have a cubic unit cell but with a tetragonal symmetry corresponding to the t′′-form.

In the following and considering the fact that all nanopowders exhibit cubic or pseudo-cubic phases at high temperature, we will name the high temperature phase as a cubic phase (or c) for every composition and crystallite average size.

3.3. Phase transitions in ZrO_2-10 mol% Sc_2O_3

The relevant transition to be studied for ZrO_2-10 mol% Sc_2O_3 nanopowders, under heating conditions, is the transformation of the volume fraction of rhombohedral β phase at low temperature to a c phase at high temperatures, with the fraction of c phase at room temperature remaining invariant.

The fraction of c phase was determined as a function of temperature, within the 400–900 °C range, by analyzing many S-XPD patterns over a narrow 2θ range close to the 111 Bragg peak of the c phase. Fig. 2a, b and c show the S-XPD patterns corresponding to ZrO_2-10 mol% Sc_2O_3 samples with three average crystallite sizes, namely $<D>$ = 35, 60 and 100 nm, respectively. The S-XPD patterns displayed in Fig. 2a, b and c were determined during the cooling process. In these three cases, the 111 peak associated to the high-temperature c phase progressively splits into two peaks of the rhombohedral β phase. The inverse transformation was also characterized by analyzing the S-XPD results corresponding to the heating cycle.

From the analysis of the measured S-XPD patterns, the weight fractions of the c and β phases were determined as functions of the temperature. The weight percentages of the c phase are displayed as hysteresis loops in Fig. 2d, e and f, for powders with average crystallite sizes $<D>$ = 35, 60 and 100 nm, respectively, under heating and cooling conditions. A first analysis of the different hysteresis loops displayed in Fig. 2d, e and f indicates that both the observed transition temperatures and the undercooling effects are size dependent. In the particular case of the nanopowder with $<D>$ = 35 nm, the on heating transformation from β to the c phase starts at 490 °C and ends at 610 °C, with 100 wt% c phase. Inversely, during the cooling cycle, the β phase becomes visible at 500 °C and reaches the final weight fraction (56 wt%) at 400 °C, the remaining 44 wt% fraction being invariant over the whole temperature cycle.

A common feature of the heating and cooling cycles of the hysteresis loops shown in Fig. 2d, e and f is the nearly zero slope of the phase fractions at low and at high temperatures. This implies that the whole phase transition is completed over the temperature ranges selected for all powders with different average crystallite size, so above this temperature range no further phase transition is expected to occur.

3.4. Phase transitions in ZrO_2-12 mol% Sc_2O_3

The availability of S-XPD patterns at room temperature over a wide 2θ range enabled us to determine the weight fractions of the c, β and γ phases by Rietveld refinements.[19] In contrast, during the heating and cooling cycles, the S-XPD patterns were recorded only over a small 2θ range close to the 111 or 220 Bragg peaks of the c phase. Therefore, for the 12 mol% Sc_2O_3 nanopowders, we have only determined the temperature dependence of the c phase content, while the intensities of the peaks corresponding to the γ and β phases were monitored as a function of temperature to analyze the β–c and γ–c transformations. Since we did not obtain any reference XPD patterns for pure β and γ phases, the temperature dependence of the fractions of the two rhombohedral phases could not be quantitatively determined by the single line method.

For ZrO_2-12 mol% Sc_2O_3 nanopowders, the relevant transition, under heatings, is the transformation from the low temperature rhombohedral β and γ phases to the high temperature c phase. Fig. 3a, b and c show the S-XPD patterns over a narrow 2θ range close to the 220 Bragg peaks corresponding to the cooling process, and associated to the different average crystallite sizes, namely $<D>$ = 35, 60 and 90 nm, respectively. The total weight fraction of the c phase as a function of temperature is displayed in Fig. 3d, e and f for nanopowders with crystallite sizes of $<D>$ = 35, 60 and 90 nm, respectively. At 400 °C, the lowest temperature of these hysteresis loops, these samples contain c, β and γ phases, with decreasing weight fractions of the c phase for increasing average crystallite size. We can notice in Fig. 3d, e, and f that the final fraction of the high temperature c phase is reached through a complex transformation including both β–c and γ–c transformations, the γ–c transition being completed at higher temperatures, above 600 °C.

3.5. Phase transitions in ZrO_2-14 mol% Sc_2O_3

At room temperature, ZrO_2-14 mol% Sc_2O_3 nanopowders with average crystallite sizes $<D>$ = 65 and 105 nm are binary mixtures of rhombohedral β and γ phases, while the sample with $<D>$ = 40 nm is also a binary mixture but, in this case, it contains c and γ phases. The sequence of on cooling S-XPD patterns close to the 220 Bragg peak corresponding to solid solutions with $<D>$ = 40, 65 and 105 nm are plotted in Fig. 4a, b and c, respectively. The analysis of these S-XPD patterns indicates that at the lowest temperature (T = 500 °C) all samples mainly contain the γ phase, with minor fractions of β phase in samples with average crystallite sizes $<D>$ = 65 and 105 nm. In the powder with the smallest crystallite sizes, $<D>$ = 40 nm, the weight fraction of c phase at 500 °C is close to 50 wt%, while in those with larger $<D>$ the c phase is absent.

Since in ZrO_2-14 mol% Sc_2O_3 nanopowders the weight fraction of the β phase at room temperature is rather small

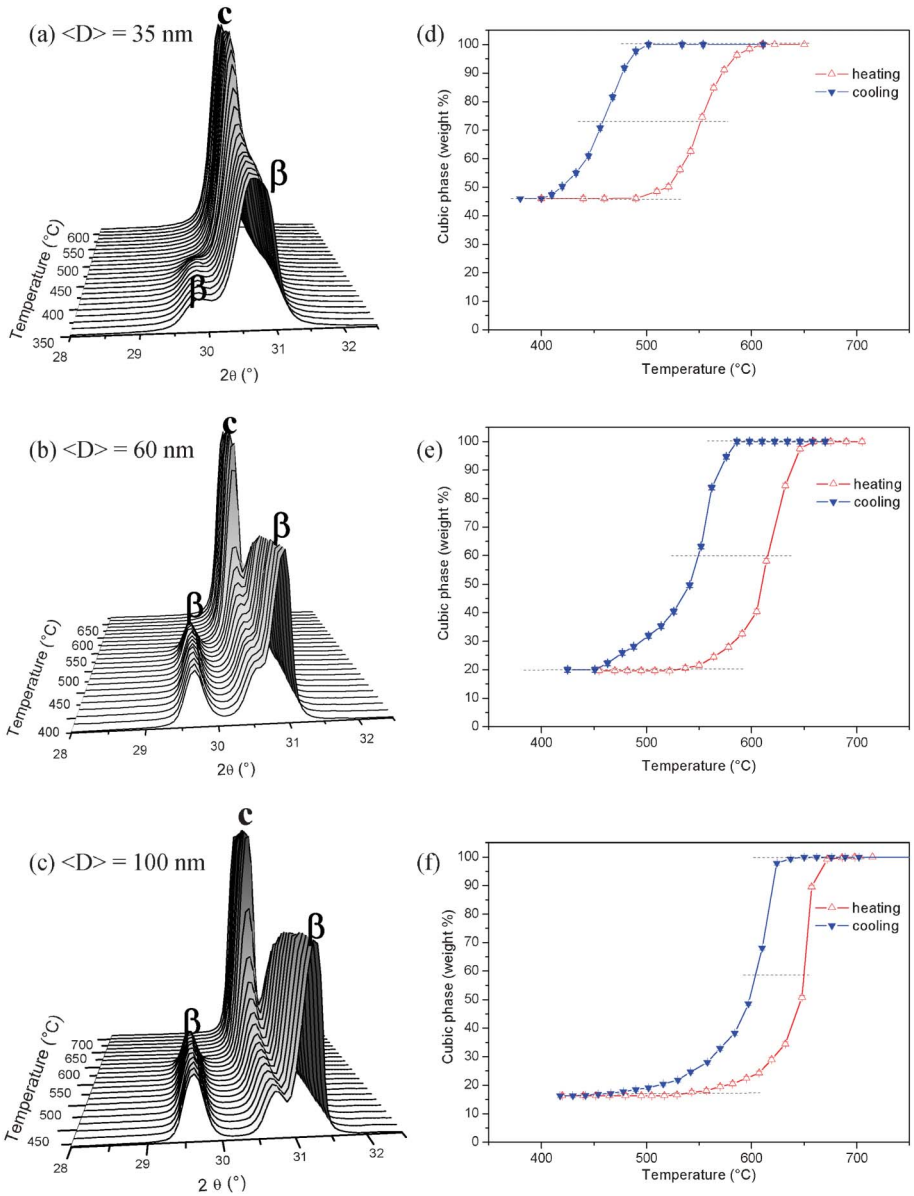

Fig. 2 S-XPD patterns for ZrO_2-10 mol% Sc_2O_3 nanopowders as functions of temperature during a cooling cycle for different average crystallite sizes, (a) $<D>$ = 35 nm, (b) $<D>$ = 60 nm and (c) $<D>$ = 100 nm. (d), (e) and (f) display the weight fractions of the cubic phase as functions of temperature, on heating and on cooling, for different average crystallite sizes, 35 nm, 60 nm and 100 nm, respectively.

(Table S1), we have considered that the relevant transition predominantly involves the rhombohedral γ and c phases. In this case the beginning and the end of the hysteresis loops plotted in Fig. 4d, e and f corresponding to average crystallite sizes $<D>$ = 40, 65 and 105 nm, respectively, are not as clear as those corresponding to other compositions. Furthermore, the overlapping of the c and γ Bragg peaks yields a higher error in the determination of the phase content. In spite of this difficulty, we have estimated the temperatures at which 50 wt% of the transformation occurs and then determined the γ–c transition temperatures, on heating and on cooling, as was previously done for the 10 mol% Sc_2O_3 samples.

Fig. 4e and 4f, corresponding to 14 mol% Sc_2O_3 nanopowders with average crystallite sizes $<D>$ = 65 and 105 nm, respectively show a double hysteresis loop. The larger loop located above 700 °C corresponds to the γ–c and the smaller one below 650 °C to the β–c transitions. In the case of 14 mol% Sc_2O_3 nanopowders with $<D>$ = 65 nm, the weight fractions at room temperature of phases β and γ are 12 and 88 wt%, respectively, these two phases transforming each of them, on heating, to the c phase at a different temperature.

The large difference in the fractions of β and γ phases in these nanopowders at room temperatures explains the observed difference in the areas of the hysteresis loops shown in Fig. 4e. Since the nanopowder with $<D>$ = 105 nm contains approximately the same proportions of β and γ phases as the sample with $<D>$ = 65 nm, a similar double hysteresis loop is also apparent (Fig. 4f). Contrarily, a double loop is not observed in

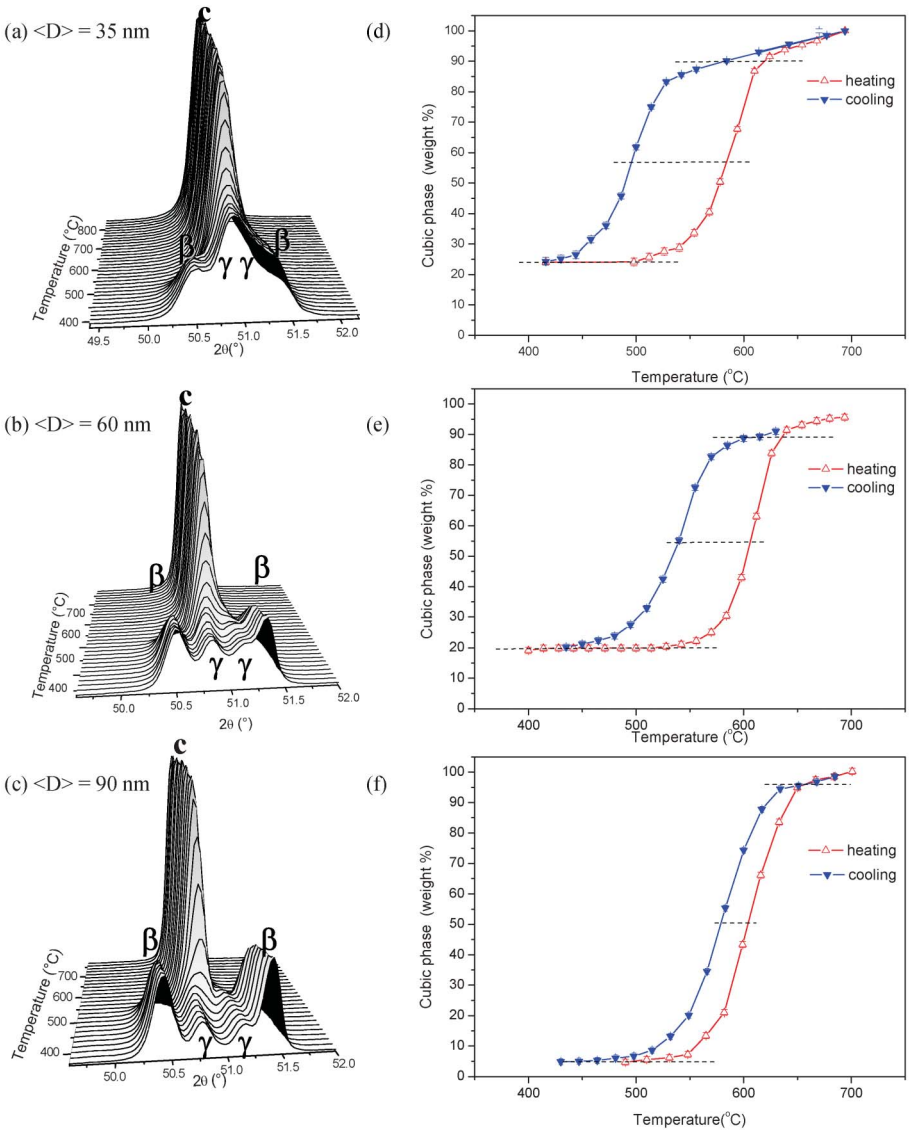

Fig. 3 S-XPD patterns for ZrO_2-12 mol% Sc_2O_3 nanopowders as functions of temperature during a cooling cycle for different average crystallite sizes, (a) $<D>$ = 35 nm, (b) $<D>$ = 60 nm and (c) $<D>$ = 90 nm. (d), (e) and (f) display the weight fractions of the cubic phase as functions of temperature, on heating and on cooling, for different average crystallite sizes, 35 nm, 60 nm and 90 nm, respectively.

Fig. 4d, corresponding to $<D>$ = 40 nm, because in this case the β phase was not detected at room temperature.

4. Discussion

This study aimed at the characterization of the main size-dependent features associated to rhombohedral–cubic phase transitions, on heating and on cooling, of ZrO_2–Sc_2O_3 nanopowders with three different Sc_2O_3 contents, namely 10, 12 and 14 mol%, and average crystallite sizes between 35 and 105 nm.

The studied transitions are characterized by a large difference between onset and ending temperatures as well as by a thermal hysteresis between the cooling and heating processes, in agreement with studies performed on bulk ZrO_2–Sc_2O_3 materials in this range of composition. In particular, the β–c phase transition has been extensively investigated in the literature for bulk materials and it has been characterized as first order and of martensitic type. The γ–c is also a first order transition, exhibits hysteresis effects and its transition temperature is higher than that of the β–c transition.[15,16]

The non-negligible width of the size distribution of the as-synthesized nanostructured powder can strongly affect the temperature width of the transition range, by decreasing and by increasing the onset and ending temperatures, respectively. In order to overcome this issue, we have considered that the temperature for which 50 wt% of the transition occurs is the transition temperature corresponding to crystallites having the average size, either on warming or on cooling.

The solid state transformation in ZrO_2-10 mol% Sc_2O_3 samples involves a simple transition from a pure single phase (rhombohedral β) to another single phase (c or t′′), on heating. Therefore, for the three studied samples with this composition, corresponding to average crystallite sizes $<D>$ = 35, 60 and 100 nm, we have precisely determined the start and the end of

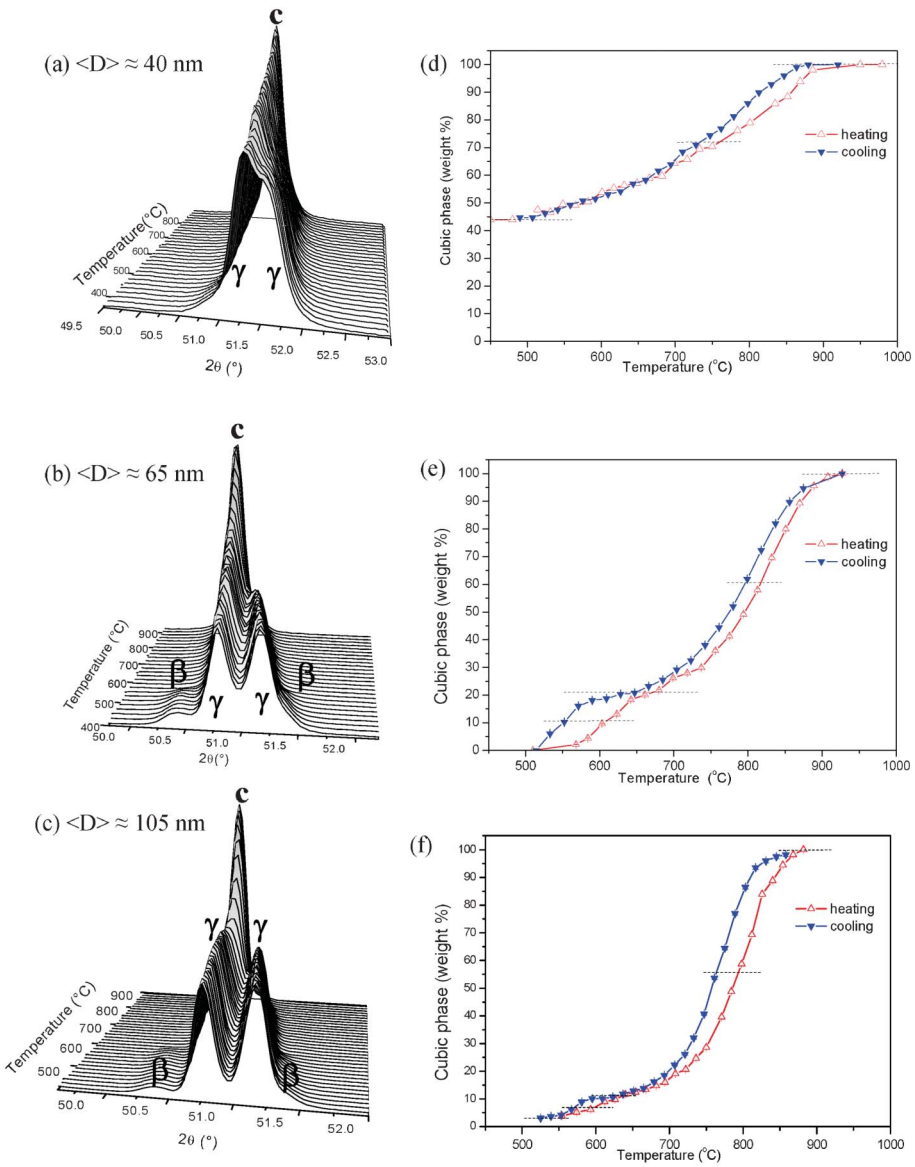

Fig. 4 S-XPD patterns for ZrO_2-14 mol% Sc_2O_3 nanopowders as functions of temperature during a cooling cycle for different average crystallite sizes, (a) $<D>$ = 40 nm, (b) $<D>$ = 65 nm and (c) $<D>$ = 105 nm. (d), (e) and (f) display the weight fractions of the cubic phase as functions of temperature, on heating and on cooling, for different average crystallite sizes, 40 nm, 65 nm and 105 nm, respectively.

the phase transition, on heating and on cooling. The determined transition temperatures in ZrO_2-10 mol% Sc_2O_3 with $<D>$ = 100 nm are observed to be close to those reported by Fujimori *et al.* for bulk samples of the same composition.[17]

For the other compositions, 12 and 14 mol% Sc_2O_3, the start and the end of the hysteresis loops were approximately estimated. Once these temperatures were established, the temperatures at which 50 wt% of the transformation occurs, on heating and on cooling, were determined and considered as the transition temperatures corresponding to the crystallites with the average size. The transition temperatures of crystallites with sizes smaller and larger than the average are expected to be slightly lower and higher, respectively, than those of crystallites with the average size.

The relevant features of the β–c transition were characterized from the phase fractions experimentally determined as a function of the temperature for 10 and 12 mol% Sc_2O_3 nanopowders and displayed in Fig. 2 and 3, respectively.

The temperatures corresponding to β–c and to γ–c transitions, on heating and on cooling, determined as previously described, are plotted in Fig. 5a. The transition temperatures determined for 12 and 14 mol% Sc_2O_3 nanopowders are not, in this case, very accurate because parts of their hysteresis loops contain the combined effects of both transformations, namely β–c and γ–c. We notice in Fig. 5a that the temperatures of the β–c and c–β transitions decrease for decreasing average crystallite size. This size effect is not clearly apparent for the transition temperatures of the γ–c transition, which were determined from the analysis of the main hysteresis loop corresponding to the 14 mol% Sc_2O_3 nanopowders. In order to explain this difference further studies that include surface energy determinations, additional S-XPD in

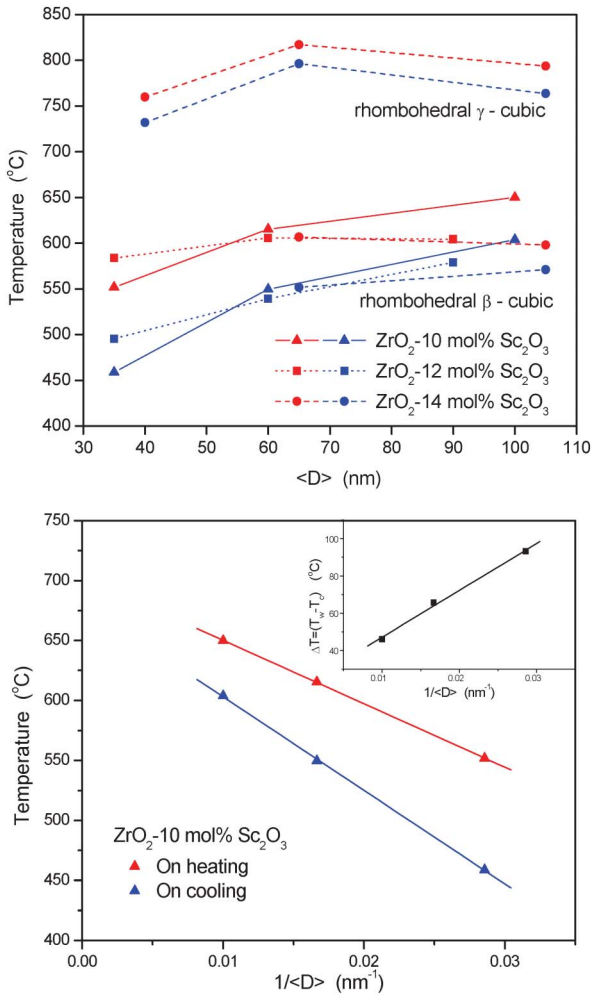

Fig. 5 On heating (red symbols) and on cooling (blue symbols) transition temperatures. (a) β-cubic and γ-cubic transition temperatures as functions of the average crystallite size, $<D>$. (b) β-cubic transition temperatures corresponding to ZrO_2-10 mol% Sc_2O_3 nanopowders as functions of $1/<D>$. Inset: difference, $(T_h - T_c)$, associated to undercooling effects.

samples with narrower size distributions and theoretical calculations are needed.

For a simple phase transition such as β–c, the dependence of the transition temperature on the average size of the assumed spherical crystallites, $T(<D>)$, is expected to be described by the Couchman–Jesser equation, eqn (1):

$$T_{\beta-c}\langle D\rangle = T_b\left[1-\frac{6\left(\frac{\sigma_\beta}{\rho_\beta}-\frac{\sigma_c}{\rho_c}\right)}{H_m\langle D\rangle}\right] \quad (1)$$

where T_b is the transition temperature corresponding to bulk crystallites, σ_β and σ_c are the surface energies of crystallites of the β and c phases, respectively, ρ_β and ρ_c are the mass densities of the β and c phases, respectively, and H_m is the transition enthalpy per unit mass for the β–c transition.[27]

Garvie *et al.* explained the retention of the tetragonal phase in nanostructured ZrO_2 on an analogous thermodynamic equation and considering that there is a difference in the surface energy between the high and the low temperature polymorphs, which is lower for the high temperature polymorph (energy difference theory).[6] Several authors have studied the crystallite size dependence of the monoclinic–tetragonal phase transition temperatures in nanostructured ZrO_2 and doped ZrO_2.[1,7,21,22] Many experimental results agree with the fact that the decreases of the stability of the tetragonal phase derives from the lower surface energy of that phase, which dominates the free energy at small particle sizes.

In order to quantitatively verify the validity of eqn (1), we have analyzed the experimental results corresponding to 10 mol% Sc_2O_3 nanopowders, for which a simple single β–c transition occurs. The transition temperatures experimentally determined on heating (β–c) and on cooling (c–β) were plotted as functions of $<D>^{-1}$ in Fig. 5b. We notice that the $T_{\beta-c}$ transition temperature exhibits a decreasing trend and a linear dependence on $<D>^{-1}$, as predicted by the Couchman–Jesser eqn (1). The temperature corresponding to the reverse c–β phase transition also exhibits a linear behavior but with a higher slope. The width of the hysteresis loop of the c–β transition, $\Delta T = T_{\beta-c} - T_{c-\beta}$, displays an increasing trend for decreasing average crystallite size. This suggests an influence of the crystallite size on the nucleation of the phases.[2]

5. Conclusions

The characteristic temperatures of the transitions from β to c phases, on heating, and from c to β phases, on cooling, were determined for ZrO_2–Sc_2O_3 nanopowders with compositions ZrO_2-10 and 12 mol% Sc_2O_3 and average crystallite sizes between 35 and 105 nm. Additionally, the temperatures corresponding to the γ–c and reverse c–γ transitions were determined for nanopowders with 14 mol% Sc_2O_3 and similar average crystallite sizes. Well-defined size dependence, with the transition temperatures decreasing for decreasing average crystallite size, was established for the β–c and c–β phase transitions, while no clear trend was observed for the γ–c and c–γ transitions.

We have demonstrated that, for this particular composition, the transition temperatures in ZrO_2-10 mol% Sc_2O_3 under heating and cooling conditions are decreasing and linear functions of $<D>^{-1}$. This result indicates that, for both the β–c and the reverse c–β transitions, the size dependences of the transition temperatures are well described by the classical Couchman–Jesser equation.

Finally, these findings have important technological relevance because the presence of low-conductivity rhombohedral phases at low temperatures, below 600 °C, is one of the main obstacles to achieve a wider application of ZrO_2–Sc_2O_3 as solid electrolytes for IT-SOFCs.

Acknowledgements

We acknowledge the financial support provided by Brazilian Synchrotron Light Laboratory (LNLS, Brazil, proposals D10B-XPD-7296 and 9195), CNPq (Brazil, PROSUL programs 490289/2005-3 and 490580/2008-4), Agencia Nacional de Promoción Científica y Tecnológica (Argentina, PICT 2005 No. 38309, PICT 2007 No. 01152 and PAE-PICT 2007 No.

02288), CONICET (Argentina, PIP No. 6559), FAPESP (Brazil) and Latin-American Centre for Physics.

References

1 M. J. Mayo, A. Suresh and W. D. Porter, *Rev. Adv. Mater. Sci.*, 2003, **5**, 100.
2 U. Donev, R. Lopez, L. C. Feldman and R. F. Haglund Jr., *Nano Lett.*, 2009, **9**, 702.
3 K. Zhu, M. S. Zhang, Y. Deng and J. Zhou, *Phys. B*, 2010, **405**, 1388.
4 P. L. Chang, Y. C. Chun, S. J. Lai and F. S. Yen, *J. Eur. Ceram. Soc.*, 2009, **29**, 3341.
5 K. R. Zhu, M. S. Zhang, J. M. Hong and Z. Yin, *Mater. Sci. Eng., A*, 2005, **403**, 87.
6 R. C. Garvie, *J. Phys. Chem.*, 1978, **82**, 218.
7 P. Bouvier, E. Djurado, C. Ritter, A. J. Dianoux and G. Lucazeau, *Int. J. Inorg. Mater.*, 2001, **3**, 647.
8 D. Prabhu, A. Narayanasamy, K. Shinoda, B. Jeyadeven, J. M. Greneche and K. Chattopadhyay, *J. Appl. Phys.*, 2011, **109**, 013532–1.
9 J. F. Q. Rey, F. F. Ferreira and E. N. S. Muccillo, *Solid State Ionics*, 2008, **179**, 1029.
10 D. Alloyeau, C. Ricolleau, C. Mottet, T. Oikawa, C. Langlois, Y. Le Bouar, N. Braidy and A. Loiseau, *Nat. Mater.*, 2009, **8**, 940.
11 Y. L. Zhang, X. J. Jin, Y. H. Rong, T. Y. Hsu (Xu Zuyao), D. Y. Jiang and J. L. Shi, *Mater. Sci. Eng. A*, 2006, **438–440**, 399.
12 M. Dapiaggi, F. Maglia, I. Tredici, B. Maroni, G. Borghini and U. A. Tamburini, *J. Phys. Chem. Solids*, 2010, **71**, 1038.
13 M. Yashima, M. Kakihana and M. Yoshimura, *Solid State Ionics*, 1996, **86–88**, 1131.
14 S. P. S. Badwal, F. T. Ciacchi and D. Milosevic, *Solid State Ionics*, 2000, **136–137**, 91.
15 H. Fujimori, M. Yashima, M. Kakihana and M. Yoshimura, *J. Appl. Phys.*, 2002, **91**, 6493.
16 P. Simoncic and A. Navrotsky, *J. Am. Ceram. Soc.*, 2007, **90**, 2143.
17 H. Fujimori, M. Yashima, M. Kakihana and M. Yoshimura, *J. Am. Ceram. Soc.*, 1998, **81**, 2885.
18 P. M. Abdala, D. G. Lamas, M. C. A. Fantini and A. F. Craievich, *J. Alloys Compd.*, 2010, **495**, 561.
19 P. M. Abdala, A. F. Craievich, M. C. A. Fantini, M. L. A. Temperini and D. G. Lamas, *J. Phys. Chem. C*, 2009, **113**, 18661.
20 P. M. Abdala, D. G. Lamas, M. C. A. Fantini and A. F. Craievich, *Phys. Chem. Chem. Phys.*, 2010, **12**, 2822.
21 F. Boulc'h and E. Djurado, *Solid State Ionics*, 2003, **157**, 335.
22 T. Chraska, A. H. King and C. C. Berndt, *Mater. Sci. Eng., A*, 2000, **286**, 169.
23 F. Furlán Ferreira, E. Granado, W. Carvalho Jr., S. Kycia, D. Bruno and R. Droppa Jr., *J. Synchrotron Radiat.*, 2006, **13**, 46.
24 D. B. Cullity, *Elements of X-ray Diffraction*, Addison-Wesley publishing Company Inc, Massachusetts, 1959, second printing.
25 J. Rodriguez-Carvajal, *Phys. B*, 1993, **192**, 55.
26 R. Pielaszek, *J. Alloys Compd.*, 2004, **382**, 128.
27 P. R. Couchman and W. A. Jesser, *Nature*, 1980, **269**, 1695.